# The (111) Surface of NaAu$_2$: Structure, Composition, and Stability

Emma J. Kwolek,[†] Roland Widmer,[‡] Oliver Gröning,[‡] Okan Deniz,[‡] Holly Walen,[†] Chad D. Yuen,[†,§] Wenyu Huang,[†] Deborah L. Schlagel,[⊥] Mark Wallingford,[⊥] and Patricia A. Thiel*,[†,⊥,∥]

[†]Department of Chemistry and [∥]Department of Materials Science & Engineering, Iowa State University, Ames, Iowa 50011, United States

[‡]nanotech@surfaces Laboratory, EMPA, Swiss Federal Laboratories for Materials Science and Technology, Ueberlandstrasse 129, 8600 Duebendorf, Switzerland

[⊥]The Ames Laboratory, Ames, Iowa 50011, United States

ABSTRACT: The (111) surface of single-crystal NaAu$_2$ is a model for catalytically active, powdered NaAu$_2$. We prepare and characterize this surface with a broad suite of techniques. Preparation in ultrahigh vacuum consists of the traditional approach of ion bombardment (to remove impurities) and thermal annealing (to restore surface order). Both of these steps, however, cause loss of sodium (Na), and repeated treatments eventually trigger conversion of the surface and near-surface regions to crystalline gold. The bulk has a limited ability to repopulate the surface Na. Under conditions where Na depletion is minimized, electron diffraction patterns are consistent with the bulk-terminated structure, and scanning tunneling microscopy reveals mesa-like features with lateral dimensions of a few tens of nanometers. The tops of the mesas do not possess fine structure characteristic of a periodic lattice, suggesting that the surface layer is disordered under the conditions of these experiments.

30nm
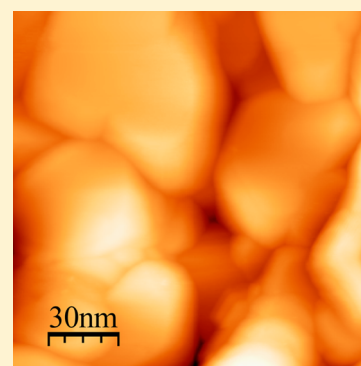
1. INTRODUCTION

Intermetallics are used commercially in a variety of applications, from structural components in the aerospace and automotive industries to energy storage devices, heating elements, and electronic materials.[1] In recent years, they have also come into consideration as possible alternatives to precious metal catalysts for certain reactions, notably steam reforming of methanol[2] and selective dehydrogenation of alkynes.[3,4] Independently, there has been great interest in gold (Au)—in the form of nanoparticles—as an effective low-temperature catalyst, especially for the benchmark reaction of CO oxidation.[5–7] These two trains of thought naturally intersect at the possibility that intermetallics containing Au might show interesting catalytic properties. John Corbett pioneered the use of Au to create diverse intermetallic compounds, and so this topic is a fitting vehicle to pay homage to his achievements in this special issue.

Recently, a simple Au-rich intermetallic, NaAu$_2$, was found to have high catalytic activity for CO oxidation at relatively low temperature ($T < 400$ K), in powdered form.[8] An explanation was proposed, on the basis of density functional theory (DFT). The theoretical work showed that the (111) surface is most stable among the low-index faces and that it is nearly bulk-terminated in its clean state. For the oxidation reaction mechanism, DFT revealed a pathway in which molecular O$_2$ triggers a Na atom to "pop out" toward the surface and then reacts with CO to form an OOCO intermediate, with subsequent dissociation to CO$_2$ as the rate-limiting step. However, experimental determination of the clean surface structure and composition—especially their relation to the bulk structure and composition—has not been undertaken. This

would test the DFT model for the catalytic surface. Thermal stability of any surface state is also an open question. The purpose of this work is to address these issues. We use a single-crystal sample to investigate the structure, composition, and stability of NaAu$_2$(111) in ultrahigh vacuum. Single crystals are advantageous because their surfaces usually exhibit a terrace—step morphology, in which the atomic arrangement on the terraces and the step heights can be compared with those in the bulk structure.[9]

No surfaces of bulk NaAu$_2$ have been characterized before, although a closely related system has been investigated. Barth et al. studied sodium (Na) films deposited on Au(111). They found that Na and Au react to form films and multilayers of NaAu$_2$, exhibiting a (111) surface orientation commensurate with the underlying Au, after heating samples (with sufficiently high Na coverages) to temperatures ranging from 300 to 600 K.[10,11]

NaAu$_2$ has a cubic unit cell with 24 atoms and a lattice parameter of 0.795 nm.[12,13] It is a diamond lattice in which four of the Na atoms fill tetrahedral holes. The (111) surface has a hexagonal arrangement of Au atoms in which $^1/_4$ of the Au atoms are missing, with a Na atom below each Au vacancy. This is represented schematically in Figure 1. The surface lattice parameter of NaAu$_2$(111) is 0.550 nm, slightly less than twice the value of 0.288 nm for Au(111). Bulk NaAu$_2$ melts congruently at 1275 K.[13]
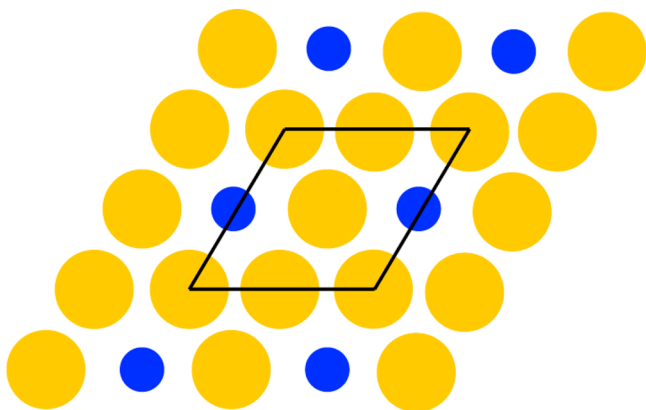
Figure 1. Schematic of the (111) plane of $NaAu_2$. Large (gold) circles represent in-plane Au atoms. Small (blue) circles represent Na atoms slightly below the surface plane. The rhombus shows the surface unit cell.

2. EXPERIMENTAL DETAILS

Single-crystal samples of $NaAu_2$ were grown at the Materials Preparation Center of The Ames Laboratory via the Bridgman technique. Special precautions were necessary to handle Na because of its sensitivity to air and moisture and its inability to be arc-melted. Special techniques were also needed to extract, cut, and polish a sample after growth because the intermetallic was brittle, and it had become bonded to the tantalum crucible, which also became brittle during growth. To our knowledge, this is the first growth of a macroscopic single crystal of this material. The sample was oriented by back-reflection Laue and the surface prepared by normal metallographic techniques because the Na was passivated once alloyed.

UHV experiments were conducted on four different samples (A–D), cut from two ingots prepared in separate growths (A from one growth and B–D from the other). The areal dimensions of the samples ranged from 2.5 to 3.5 mm in width and from 5.5 to 9.5 mm in length. Different sets of experiments were carried out on different samples, with some overlap. Two of the samples were repolished during the course of the experiments, and this was considered to produce a totally fresh surface of $NaAu_2$, based on data presented in section 3.1. From this combined and extensive data set, certain trends emerged, which are reported in section 3.

Experiments were conducted both at EMPA in Dübendorf, Switzerland, and at The Ames Laboratory in Ames, IA. All of the X-ray photoelectron diffraction (XPD) and low-energy electron diffraction (LEED) experiments were carried out at EMPA, together with the majority of the scanning tunneling microscopy (STM) and X-ray photoelectron spectroscopy (XPS) work. Some STM and XPS, plus all of the temperature-programmed desorption (TPD) and X-ray diffraction (XRD) work was done at The Ames Laboratory. Details relevant to the EMPA work[14] and to the Ames work[15] are available elsewhere.

All experiments (except XRD and TPD) were done in UHV with base pressure below 1.0×10^{-10} mbar. TPD was carried out in UHV with a base pressure of 7×10^{-10} mbar. XRD was conducted in air. All data were acquired with the sample at room temperature, except, of course, in TPD.

After introduction to UHV and between each experiment, each sample was sputtered and annealed. Typically, sputtering was done with 0.75 keV Ar^+ for 5 min at normal incidence and with the sample at 300 K. Annealing temperatures of 435–850 K were investigated, and the most common annealing condition was 20 min at 500 K.

In XPS and XPD, an Al $K\alpha$ source was used. XPS data were analyzed using *CASA* software.[16] Sensitivity factors for Na and Al were 8.52 and 17.1, respectively. In XRD, θ/θ scans were measured using Co $K\alpha$ radiation (1.79 Å) and a PANalytical X'Pert Pro system. The XRD data were used purely for phase analysis.

3. EXPERIMENTAL RESULTS

3.1. Composition from XPS and XRD. Figure 2 shows the Na/Au composition ratio, R, as a function of the number of sputtering—
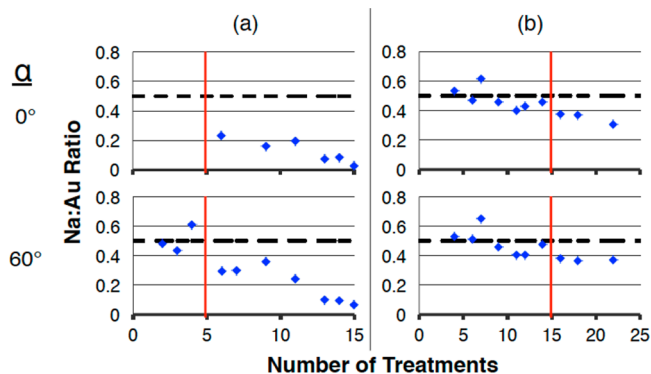

Figure 2. Na/Au composition ratio, from XPS, as a function of the treatment in UHV. XPS data were not acquired after every treatment, so the number of data points is less than the number of treatments. The compositions are derived from the relative intensities of the Na 1s and Au 4f lines in XPS, as described in section 2. (a) Evolution of sample A. This sequence encompassed a wide variety of T_{ann} values from 430 to 770 K. Prior to Na depletion, the treatments included two at T_{ann} = 600 K and one at T_{ann} = 650 K. (b) Evolution of sample B. Each treatment included annealing at 500 K for 20 min. The top two panels show the results for normal emission ($\alpha = 0°$), while the bottom two panels show grazing emission ($\alpha = 60°$).

annealing treatments for two samples. (Between each treatment, an experiment such as XPD or STM was conducted.) Both samples showed ratios close to that expected from the bulk stoichiometry, R = 0.5, up to the point marked by the vertical line. For treatments to the right of the line, R dropped below 0.4 and never recovered.

The sample in Figure 2a was annealed at temperatures (T_{ann}) of 430–600 K up through treatment 4 (just to the right of the vertical line), where it was annealed at T_{ann} = 650 K. This sequence, involving some treatments at relatively high T_{ann}, apparently triggered a permanent depletion of Na. The sample in Figure 2b was kept at a lower T_{ann} of 500 K. Nonetheless, its composition changed permanently after treatment 15. When R dropped below 0.4, no subsequent treatment could cause it to increase again, including long annealing periods at low T_{ann} = 430–500 K or short annealing periods at high T_{ann} = 770–850 K. Together, these results show that irreversible Na depletion in the surface and near-surface regions occurs quickly at high T_{ann} (600–650 K) or slowly as a result of sputtering—annealing cycles at lower T_{ann} (500 K). In other words, not only temperature but also cumulative history is important. In the end, our preferred UHV treatment consisted of sputtering for 5 min and annealing at 500 K for 20 min. Samples could be subjected to 12–15 of these treatments before showing a surface compositional change and other signs of irreversible Na depletion outlined in section 3.3.

Sample deterioration, resulting from repeated sputtering—annealing treatments in UHV, is confirmed by XRD of samples before or after use in UHV. Figure 3a is a powder pattern from part of a ground $NaAu_2$ crystal; only lines associated with $NaAu_2$ are visible. Parts b and c of Figure 3 are post-mortem XRD patterns of single crystals that had shown signs of Na depletion. In Figure 3b, signatures of Au and $NaAu_2$ coexist, whereas in Figure 3c, only Au is evident. Clearly, Na depletion in UHV causes conversion to bulk Au, and this conversion is more complete in Figure 3c than in Figure 3b. Further, given that XRD is sensitive to a depth of at least 1 μm, Figure 3c—showing only crystalline Au—indicates that Na depletion can penetrate to at least this depth. Figure 3d represents a single crystal that was repolished after Na depletion, whereby 0.24 mm of material was removed from the surface. Only peaks from $NaAu_2$ appear. Therefore, Na depletion is
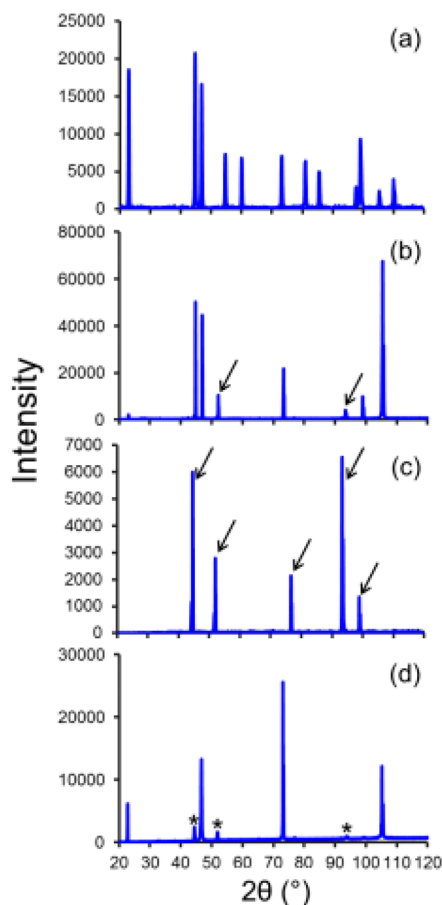
Figure 3. XRD patterns of $NaAu_2$ samples. (a) Powder pattern from a portion of the sample D ingot that was crushed and ground. All peaks are attributed to $NaAu_2$. (b) Sample A single crystal after heating from 400 to 850 K in 50 K increments with 3 min of sputtering before each heating. The Na/Au composition ratio was not measured, but these conditions are expected to produce a Na-depleted surface. The pattern is a mixture of peaks assigned to $NaAu_2$ and Au, with the latter denoted by arrows. (c) Sample D single crystal after 11 treatments that included flashing or annealing at 775 and 825 K. These conditions are expected to produce a Na-depleted surface, as confirmed by $R = 0.09$ in XPS at $\alpha = 0°$. The major XRD peaks can all be assigned to Au, denoted by arrows. (d) Sample D single crystal after repolishing, which removed 0.24 mm from the surface. All peaks are attributed to $NaAu_2$, except the small features marked by asterisks, which are from the stainless steel sample holder. These features also make very small contributions in panels b and c.

limited to the region adjacent to the surface, and a sample can be regenerated by removing this region.

In the following two sections, we first present data acquired under conditions where samples exhibited a surface composition close to that of the bulk, i.e., before irreversible Na depletion. We then return to the issue of Na depletion and its effect on the surface properties.

3.2. Surface Characterization *before* Na Depletion. *LEED.* Figure 4a shows LEED patterns that are typical of an undepleted sample. There is good agreement with the patterns expected for a bulk-terminated surface, shown in Figure 4b. Furthermore, we derive a surface lattice constant of 0.54 ± 0.02 from the LEED data, in agreement with the literature value of 0.550 nm. Thus, LEED is consistent with a bulk termination. However, the level of background intensity in the measured patterns suggests some degree of disorder.

XPD. The XPD data are illustrated in Figure 5a for the Na 1s and Au 4f lines. Corresponding single-scattering calculations are shown in Figure 5b. For both Na and Au, the symmetries and positions of the features in the pattern agree well between the experiment and
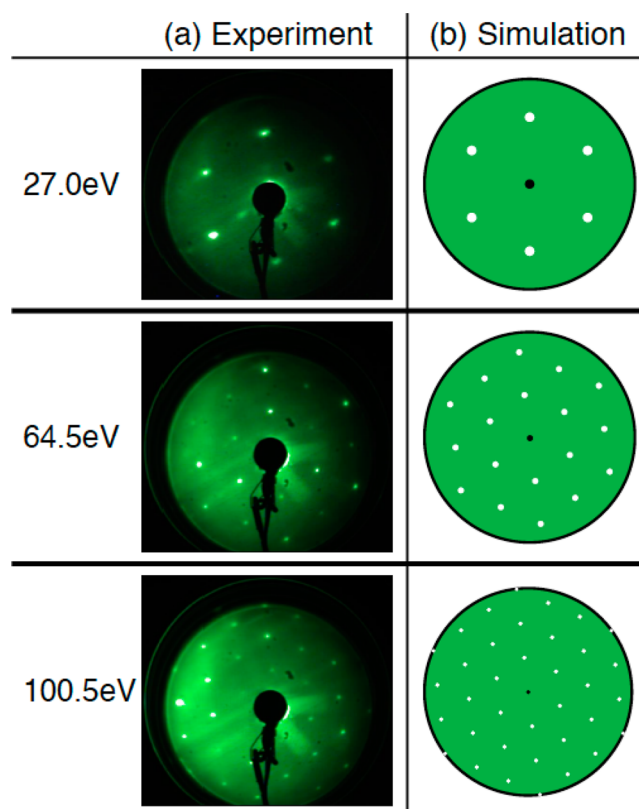

Figure 4. LEED patterns at three incident electron energies and normal incidence. (a) Sample C, after 13 sputtering—annealing treatments, resulting in a cumulative history of 3 h of sputtering and 18 h of annealing at temperatures not exceeding 530 K. $R = 0.55$ ($\alpha = 60°$). (b) LEED pattern expected for the $NaAu_2(111)$ bulk-terminated surface (Figure 1).

simulation, although the level of anisotropy (differences in amplitude between bright and dark features) for the Na 1s line does not. Note that the simulation for unreconstructed Au(111) is very similar to that for bulk-terminated $NaAu_2$, so the Au 4f pattern cannot be used to distinguish between the two types of surfaces. The similarity between simulations for the two Au models is reasonable because the surface plane of $NaAu_2(111)$ can nearly be considered a Au(111) plane in which some Au atoms are missing.

STM. Figure 6 shows that undepleted surfaces typically do not exhibit the terrace—step morphology that is characteristic of single-crystal surfaces. Rather, they show individual mesa-like features with maximum diameters of about 60 nm. The images in Figure 6 are highly representative of the undepleted $NaAu_2(111)$ surfaces. The mesas have flat tops with a peak-to-peak roughness below 0.20 nm. Despite extensive efforts, no atomic-scale features could be resolved atop the mesas. Also, there is no systematic trend in the differences between the heights of the mesas, which range from 0.1 to 8 nm. The fact that good LEED and XPD patterns can be obtained from such a surface indicates that the mesas are atomically ordered and orientationally aligned. The partial disorder reflected in LEED and XPD may result, at least in part, from the interfaces and valleys between mesas.

3.3. Surface Characterization *after* Na Depletion. *STM.* Figure 7 shows images of a surface that is deficient in Na. The majority of the surface is rough and featureless, like the image in Figure 7a. Small parts can be found, however, that exhibit the well-known herringbone reconstruction of Au(111), as shown in Figure 7b. This herringbone-decorated terrace is bordered by a step bunch in which the step height is 0.25 ± 0.01 nm. This value agrees with the bulk separation between (111) planes in Au, 0.243 nm. (Note that the measured step heights have been calibrated against known step heights on a (111) surface of
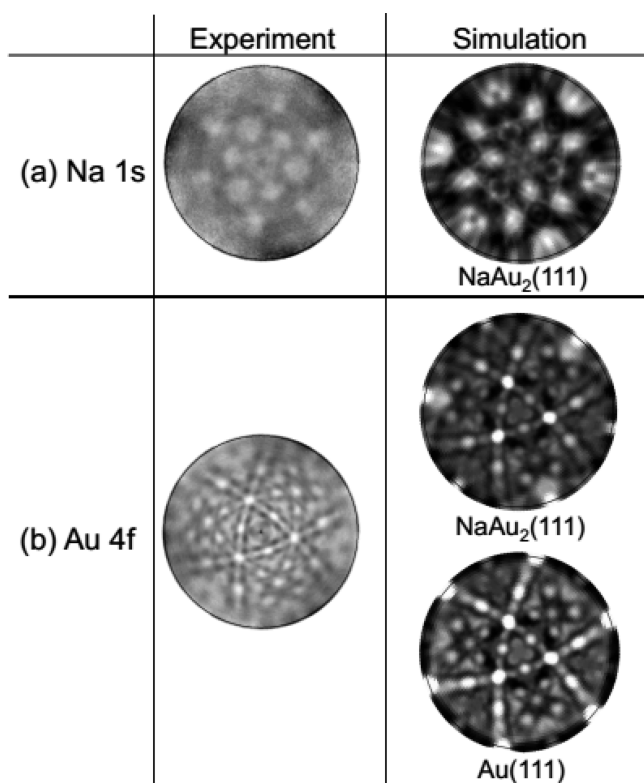
Figure 5. Comparison of experimental XPD patterns from sample B with single-scattering calculations. Before XPD measurements, the sample underwent a total of five sputtering–annealing treatments at T_{ann} = 500 K, which resulted in R = 0.53 (α = 60°). The sample was scanned at α = 0–90° in 1° steps. (a) Na 1s. (b) Au 4f.

a Au single crystal.) Similar step bunches and herringbone-decorated terraces are not uncommon on surfaces with $R \leq 0.4$.

3.4. Evidence Regarding Mechanisms of Na Depletion. Each sputtering–annealing treatment has the potential to remove Na in two
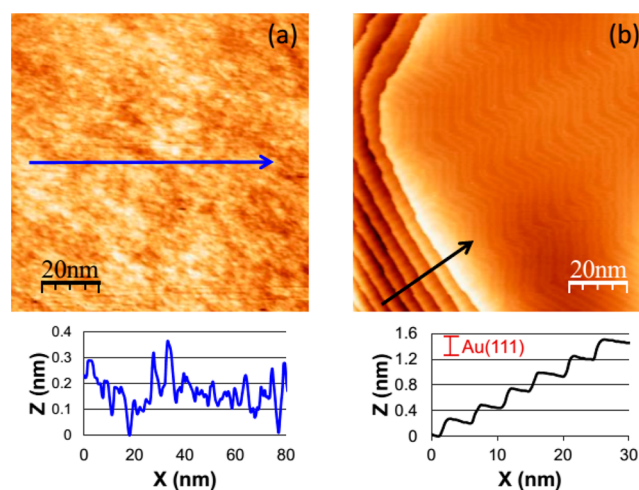

Figure 7. STM images of sample A after Na depletion, R = 0.24 (α = 60°). The sample started with a history of 10 sputtering–annealing treatments at T_{ann} = 430–750 K. Between images, it was sputtered and annealed for 20 min at 770 K. (a) Typical surface image at +0.82 V and 0.08 nA. (b) Isolated region showing the herringbone reconstruction and step height associated with Au(111) at −1.4 V and 0.08 nA. The average step height is 0.25 ± 0.01 nm.

ways: Preferential evaporation of Na during annealing and preferential removal of Na by sputtering. Our data indicate that both processes contribute.

TPD. In Figure 8, the partial pressure of Na in the gas phase (proportional to the desorption rate) is shown as a function of increasing temperature, for three different heating rates. Thermally activated desorption of Na is first detected at about 450 K. These experimental data became available after we observed Na depletion using other techniques and after we developed the protocol for sputtering–annealing that involved heating to 500 K. Thus, during the standard annealing treatment, there is continual evaporation of Na but at a moderately low rate. This explains the observation (section 3.1)
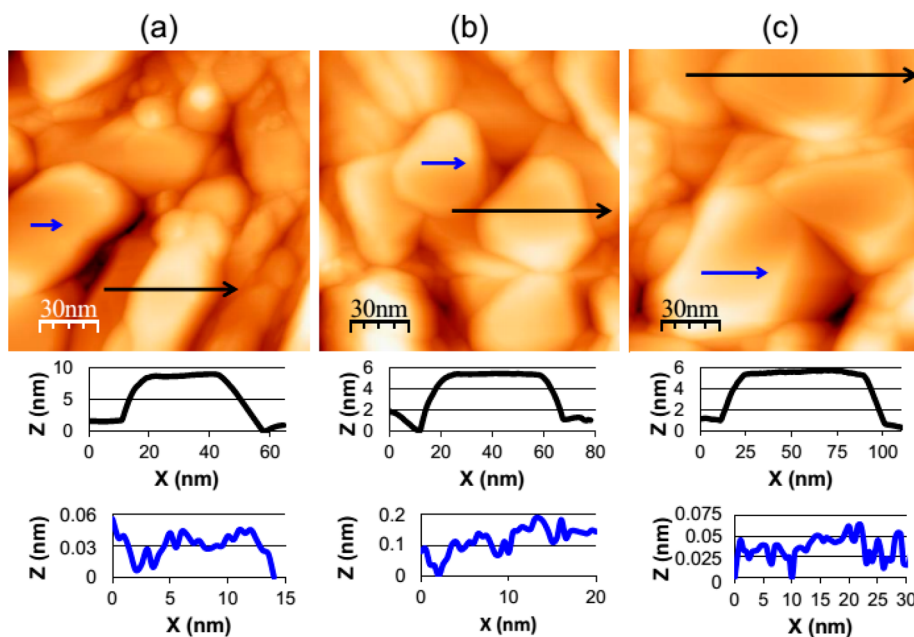
Figure 6. STM images and line profiles of sample C. The sample started with a history of eight sputtering–annealing treatments at T_{ann} = 425–480 K. Between each pair of images, it was sputtered once and annealed for 20 min 480–515 K. Values of R were measured at α = 60°. Tunneling parameters ranged from +1.1 to +1.6 V at the tip and from 0.1 to 0.3 nA. (a) R = 0.48. (b) R = 0.47. (c) R = 0.44.
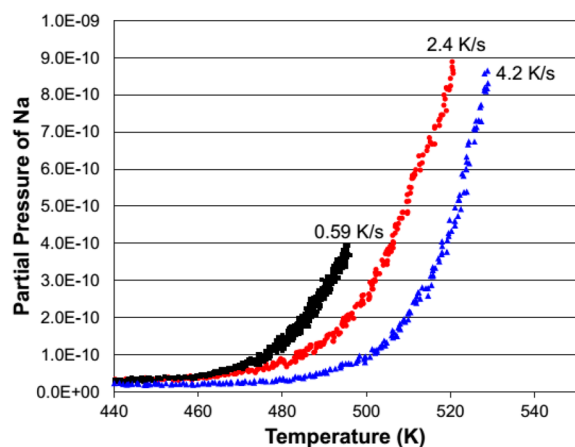
Figure 8. TPD spectra from sample D showing the partial pressure of Na (mass-to-charge ratio of 23) versus temperature. Three different heating rates were used: 0.59, 2.4, and 4.2 K/s.

that heating a sample to temperatures of 600 K or above causes rapid deterioration, while heating to 500 K causes gradual deterioration.

In the TPD curves, the highest rate of desorption of Na at a given temperature is associated with the lowest heating rate. This observation can be explained if the rate of Na desorption is affected by the rate of Na transport from the bulk to the surface. For slow heating rates, the surface and bulk remain close to equilibrium and the surface is constantly replenished, while at high heating rates, the surface Na cannot be repopulated quickly enough and desorption slows.

Preferential Sputtering. Preferential sputtering in alloys and intermetallics is a well-known phenomenon. In $NaAu_2$, Ar^+-ion sputtering reduces the Na concentration to very low levels. Data from a representative experiment are given in Table 1, for the same

Table 1. Effect of Sputtering (Alone) on the Composition of Sample B[a]

	atom % Na	atom % Au	R
initial condition	27.0	73.0	0.37
after sputtering	4.7	95.3	0.05

[a]The initial condition corresponds to treatment 22 in Figure 2b. After the initial measurement of R, the sample was sputtered again for 5 min with 0.75 keV Ar^+ ions, but it was not annealed. Then the second value of R was obtained.

sample as that in Figure 2b. The sample was initially prepared by sputtering for 5 min and annealing at 500 K, corresponding to treatment 22 in Figure 2b. After sputtering again for 5 min without subsequent annealing, R dropped to 14% of its initial value, indicating selective removal of Na.

Preferential sputtering can be attributed, in this case, to the better mass match of Ar^+ (40 amu) with Na (23 amu) than with Au (197 amu), resulting in more effective momentum transfer from the incident ion to Na than to Au. We conclude that Ar^+-ion sputtering contributes to the overall Na depletion in $NaAu_2$.

4. DISCUSSION

This work shows that the nature of the (111) surface of bulk $NaAu_2$ depends strongly on the conditions of its preparation in UHV.

If the sample is not heated too high ($T_{ann} \leq 500$ K) or subjected to excessive sputtering–annealing cycles, its surface exhibits characteristics consistent with bulk termination. This is based upon both LEED and XPD, where the measured patterns are very close to simulations based on the bulk structure. In

particular, the surface lattice constant calculated from the LEED data agrees well with the value for the bulk-terminated unit cell, and the LEED pattern contains no extra diffraction spots that might indicate surface reconstruction. However, in both techniques, some disorder is suggested by the moderately high background in the patterns.

The STM data are unusual because they do not display the anticipated terrace–step structure but rather an array of mesa-like features with diameters on the order of a few tens of nanometers. These mesas give rise to the good LEED and XRD patterns, yet no regular atomic-scale structure can be discerned on the flat (to within 0.2 nm) tops. One possible explanation is that the top atomic layer is disordered and the LEED and XRD patterns originate mainly from deeper layers. Perhaps the disorder is a static remnant of the dynamic Na desorption, which occurs at temperatures above the observation temperature of 300 K. However, Barth et al. observed good atomic-scale order on the surfaces of $NaAu_2$ films grown on Au(111) and heated to temperatures of 300–600 K.[10,11] The reason for the contradictory result is unclear, although there are certain differences between the two systems and these may be significant. For instance, in the work of Barth et al., $NaAu_2$ was in the form of a thin surface layer with significant strain, and excess Au existed in the subsurface region (the Au substrate).

It is interesting that the mesas produce good LEED and XRD patterns. This means that the mesas must be atomically ordered and orientationally aligned; i.e., their orientation is fixed by the bulk lattice. Although the STM images in Figure 6 may give the impression that the mesas are independent mounds, they are more correctly regarded as terrace-like features separated by irregular valleys and crevasses. The reason for this unusual morphology warrants further investigation.

If the sample is heated to higher temperatures ($T_{ann} \geq 600$ K) and/or subjected to many sputtering–annealing treatments at $T_{ann} \leq 500$ K, it loses Na and eventually decomposes into elemental Au at the surface and in the adjacent bulk region. Evidence for this comes from the irreversible drop in R in XPS and the emergence of bulk Au in XRD. Because a $NaAu_2$ surface can be regenerated by polishing, Na depletion must be limited to the near-surface region. In a Na-depleted sample, there are small areas that have the herringbone reconstruction of Au(111), as well as cascades of steps each having the height of a Au(111) step. Such regions are in the minority, however, and most of the Na-depleted surface simply appears rough and featureless in STM.

We have determined that two mechanisms contribute to Na depletion. Thermally activated desorption begins around 450 K. Preferential sputtering also contributes. Our model is that when surface and near-surface depletion becomes too extensive, the bulk can no longer replenish the surface effectively, and the surface transforms to Au. In fact, the importance of surface Na repopulation is evident from the inverse correlation between the Na desorption and heating rates (at fixed temperature) in TPD.

Returning to the original motivation for this work, we can comment on the plausibility of $NaAu_2$(111) as a model for the catalytically active surface. In powder form, $NaAu_2$ showed good catalytic activity for CO oxidation at temperatures of 300–350 K.[8] A reaction mechanism was proposed on the basis of the nearly bulk-terminated (111) surface. The present work does not *prove* that a (111)-like surface exists under reaction conditions, but this work is *compatible* with this model for the

catalyst operating in this temperature range. The present work also predicts massive compositional changes in the intermetallic catalyst, starting at reaction temperatures of about 450 K.

5. CONCLUSIONS

We have found that the (111) surface of $NaAu_2$ can be prepared in a state where orientationally aligned, mesa-like features predominate. This state produces good diffraction patterns in LEED and XPD, which are matched well by simulations based on a bulk-terminated structure. However, there is no regular fine structure atop the mesas, possibly indicating disorder in the topmost surface layer. The sample can lose Na both by thermal evaporation (onset at 450 K) and by Ar^+-ion bombardment. Repeated sputtering−annealing treatments under the conditions described here lead to precipitation of pure Au at the surface and near-surface regions.

■ AUTHOR INFORMATION

Corresponding Author
*E-mail: pthiel@iastate.edu.

Present Address
§C.D.Y.: Department of Chemistry and Biochemistry, Augstana College, Rock Island, Illinois 61201.

Notes
The authors declare no competing financial interest.

■ ACKNOWLEDGMENTS

■ REFERENCES

(1) Stoloff, N. S.; Liu, C. T.; Deevi, S. C. *Intermetallics* **2000**, *8*, 1313−1320.
(2) Tsai, A. P.; Yoshimura, M. *Appl. Catal., A* **2001**, *214*, 237−241.
(3) Kovnir, K.; Ambrüster, M.; Teschner, D.; Venkov, T. V.; Jentoft, F. C.; Knop-Gericke, A.; Grin, Y.; Schlögl, R. *Sci. Technol. Adv. Mater.* **2007**, *8*, 420−427.
(4) Armbrüster, M.; Kovnir, K.; Friedrich, M.; Teschner, D.; Wowsnick, G.; Hahne, M.; Gille, P.; Szentmiklosi, L.; Feuerbacher, B.; Heggen, M.; Girgsdies, F.; Rosenthal, D.; Schlögl, R.; Grin, Y. *Nat. Mater.* **2012**, *11*, 690−693.
(5) Haruta, M.; Kobayashi, T.; Sano, H.; Yamada, N. *Chem. Lett.* **1987**, *16*, 405−408.
(6) Hashmi, A. S. K.; Hutchings, G. J. *Angew. Chem.* **2006**, *45*, 7896−7936.
(7) Min, B. K.; Friend, C. M. *Chem. Rev.* **2007**, *107*, 2709−2724.
(8) Xiao, C. X.; Wang, L.-L.; Maligal-Ganesh, R.; Smetana, V.; Walen, H.; Thiel, P. A.; Miller, G. J.; Johnson, D. D.; Huang, W. *J. Am. Chem. Soc.* **2013**, *135*, 9592−9595.
(9) Thiel, P. A.; McGrath, R. In *Properties of Composite Surfaces*; Wandelt, K., Ed.; Wiley: New York, 2013.
(10) Barth, J. V.; Brune, H.; Schuster, R.; Ertl, G.; Behm, R. J. *Surf. Sci.* **1993**, *292*, L769−L774.
(11) Barth, J.; Behm, J.; Ertl, G. *Surf. Sci.* **1995**, *341*, 62−91.
(12) Lieser, K.; Witte, H. *Z. Metallkd.* **1952**, *43*, 396−401.
(13) Pelton, A. D. *Bull. Alloy Phase Diagrams* **1986**, *7*, 136−139.
(14) Rosenthal, D.; Widmer, R.; Wagner, R.; Gille, P.; Armbrüster, M.; Grin, Y.; Schlögl, R.; Gröning, O. *Langmuir* **2012**, *28*, 6848−6856.
(15) Yuen, C. D.; Miller, G. J.; Lei, H.; Wang, C.-Z.; Thiel, P. A. *J. Phys.: Condens. Matter* **2013**, *25*, 485002.
(16) *CasaXPS: Processing Software for XPS, AES, SIMS and More*, www.CasaXPS.com (Oct 19, 2014).